RADIO ASTRONOMY

Frequency-dependent polarization of repeating fast radio bursts—implications for their origin

Yi Feng[1,2,3], Di Li[1,2,4,*], Yuan-Pei Yang[5], Yongkun Zhang[1,3], Weiwei Zhu[1], Bing Zhang[6,7], Wenbin Lu[8], Pei Wang[1], Shi Dai[9], Ryan S. Lynch[10], Jumei Yao[11], Jinchen Jiang[1,12], Jiarui Niu[1,3], Dejiang Zhou[1,3], Heng Xu[1,12], Chenchen Miao[1,3], Chenhui Niu[1], Lingqi Meng[1,3], Lei Qian[1], Chao-Wei Tsai[1], Bojun Wang[1,12], Mengyao Xue[1], Youling Yue[1], Mao Yuan[1,3], Songbo Zhang[13], Lei Zhang[1]

The polarization of fast radio bursts (FRBs), which are bright astronomical transient phenomena, contains information about their environments. Using wide-band observations with two telescopes, we report polarization measurements of five repeating FRBs and find a trend of lower polarization at lower frequencies. This behavior is modeled as multipath scattering, characterized by a single parameter, σ_{RM}, the rotation measure (RM) scatter. Sources with higher σ_{RM} have higher RM magnitude and scattering time scales. The two sources with the highest σ_{RM}, FRB 20121102A and FRB 20190520B, are associated with compact persistent radio sources. These properties indicate a complex environment near the repeating FRBs, such as a supernova remnant or a pulsar wind nebula, consistent with their having arisen from young stellar populations.

Fast radio bursts (FRBs) are bright millisecond-duration astronomical transient phenomena observed in radio bands (1). Some FRBs, such as FRB 20121102A (2), are known to repeat, but it remains unclear whether repeating FRBs (hereafter "repeaters") are ubiquitous or uncommon sources. Whether all FRBs repeat on some time scale, or whether repeaters form a separate population from single-burst sources, has implications for the energy source (3), host environments (4), luminosity function (5), apparent and intrinsic event rates (6), and predicted survey yields (7).

Information about FRB hosts and environments could be obtained from their polarization. Faraday rotation is the phenomenon whereby the polarization position angle of linearly polarized radiation, propagating through a magneto-ionic medium, is rotated as a function of frequency. It is quantified by the rotation measure (RM), which carries information about the local environment and the intervening medium. The substantial and time-varying

RM of FRB 20121102A has been interpreted as due to a dynamic magneto-ionic environment (8), such as an expanding supernova remnant or a pulsar wind nebula (9, 10). The polarization position angle and fraction of linear and circular polarization could constrain the emission mechanisms (11, 12). For example, a constant polarization position angle across a burst is consistent with either a model invoking a relativistic shock, or emission from the outer magnetosphere of a neutron star (3). Alternatively, the varying polarization angle observed in the repeater FRB 20180301A has been interpreted as originating within the magnetosphere of a magnetar (a highly magnetized neutron star) (13).

In this study, we analyzed the polarization properties of 21 FRB sources, 9 of which have been confirmed to repeat. We observed five of them—FRB 20121102A, FRB 20190520B, FRB 20190303A, FRB 20190417A, and FRB 20201124A—with the Five-hundred-meter Aperture Spherical radio Telescope (FAST) and the Robert C. Byrd Green Bank Telescope (GBT). The other 16 sources were taken from the literature (table S1). Our goals were to examine their RM, linear polarization fraction, and its dependence on frequency.

The repeater FRB 20121102A has previously been precisely localized to a dwarf galaxy (2, 14). This FRB has a bimodal burst energy distribution, with 1652 independent bursts detected in 59.5 hours spanning 62 days (15). Using the same dataset, we searched RM in each of the 1652 bursts and detected no linear polarization, setting a 6% upper limit on the degree of linear polarization at 1.0 to 1.5 GHz (16). For comparison, previous observations showed almost 100% linear polarization at 3 to 8 GHz (8).

FRB 20190520B is another repeater localized to a persistent radio source (PRS) in another dwarf galaxy (17, 18). An RM search

for 75 bursts (18) resulted in no detection, with an upper limit of 20% on the degree of linear polarization at 1.0 to 1.5 GHz (16). Our follow-up observations with the GBT detected three bursts in the range of 4 to 8 GHz, with an average RM of 2759 rad/m² (16). Representative polarization pulse profiles and dynamic spectra of this source are shown in Fig. 1C.

FRB 20190303A, FRB 20190417A, and FRB 20201124A were discovered at 400 to 800 MHz (19, 20). We followed up these sources with the FAST 19-beam system at 1.0 to 1.5 GHz. From FRB 20190303A, three bursts were detected with an average RM of −411 rad/m², which help localize the source to right ascension (RA) 13ʰ51ᵐ58ˢ, declination (Dec) +48°07′20″ (J2000 equinox) with a circular 2.′6 uncertainty region (16). Compared with the earlier lower-frequency measurements (19), the RM has changed by ~100 rad/m² in 1.5 years. In contrast to the earlier low linear polarization (19), the bursts detected with FAST are nearly 100% linearly polarized.

From FRB 20190417A, we detected 23 bursts, five of which have measurable polarization with an average RM of 4681 rad/m². The estimated position of FRB 20190417A is (RA, Dec) = (19ʰ39ᵐ22ˢ, +59°18′58″) (J2000) with circular uncertainty 2.′6 (16). FAST follow-up observations of FRB 20201124A resulted in 11 bursts that were sufficiently bright to be used in our analysis (16). We also detected nine polarized bursts with the GBT at 720 to 920 MHz, with an average RM of −684 rad/m². Both FRB 20190417A and FRB 20201124A have higher linear polarization at higher frequencies.

The average RMs of each FRB are listed in table S2. The time of arrival, central frequency of the burst emission (weighted by the burst signal-to-noise ratio as a function of frequency), intrachannel depolarization f_{depol} (see below and Eq. 1), RM, and degrees of debiased (16) linear and circular polarization of each pulse are listed in table S3. Representative polarization pulse profiles and their dynamic spectra are shown in Fig. 1 (16).

The observations of these five sources all indicate decreasing linear polarization with decreasing frequencies. To explain this behavior, we consider three possible effects: (i) intrinsic frequency evolution of the linear polarization, (ii) intrachannel depolarization, and (iii) RM scatter.

Intrinsic frequency evolution of linear polarization is already known for pulsars (21). The polarization tends to decrease from lower to higher frequencies, which has been attributed to emission from different heights in the pulsar magnetospheres (22). This is the opposite trend to the one we find for repeating FRBs, so a direct analogy is not supported by the data. Given the lack of understanding of FRB origin(s), our results cannot rule out other scenarios involving pulsar-magnetosphere–like environments.

[1]National Astronomical Observatories, Chinese Academy of Sciences, Beijing 100101, China. [2]Zhejiang Lab, Hangzhou, Zhejiang 311121, China. [3]School of Astronomy and Space Science, University of Chinese Academy of Sciences, Beijing 100049, China. [4]National Astronomical Observatories, Chinese Academy of Sciences–University of KwaZulu-Natal Computational Astrophysics Centre, University of KwaZulu-Natal, Durban 4000, South Africa. [5]South-Western Institute for Astronomy Research, Yunnan University, Kunming, Yunnan 650504, China. [6]Department of Physics and Astronomy, University of Nevada, Las Vegas, NV 89154, USA. [7]Nevada Center for Astrophysics, University of Nevada, Las Vegas, NV 89154, USA. [8]Department of Astrophysical Sciences, Princeton University, Princeton, NJ 08544, USA. [9]School of Science, Western Sydney University, Penrith, NSW 2751, Australia. [10]Green Bank Observatory, Green Bank, WV 24401, USA. [11]Xinjiang Astronomical Observatory, Chinese Academy of Sciences, Urumqi, Xinjiang 830011, China. [12]School of Physics, Peking University, Beijing 100871, China. [13]Purple Mountain Observatory, Chinese Academy of Sciences, Nanjing 210023, China.
*Corresponding author. Email: dili@nao.cas.cn
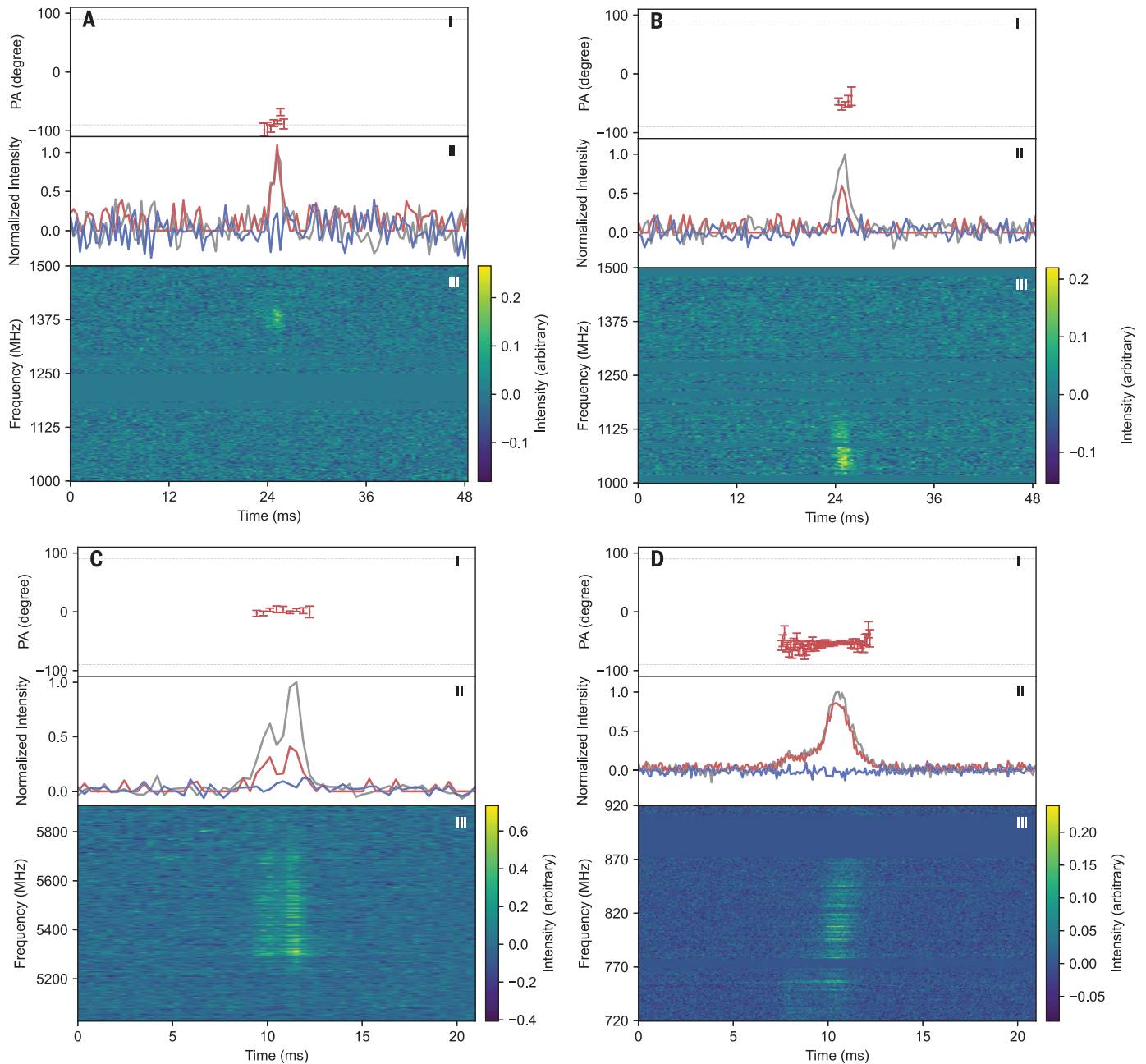
Fig. 1. Polarization position angle and intensity profiles, with dynamic spectra, for four repeating FRBs. (**A**) FRB 20190303A, (**B**) FRB 20190417A, (**C**) FRB 20190520B, and (**D**) FRB 20201124A. In each panel, the top subpanel (I) shows the polarization position angle (PA), with gray dashed lines indicating ±90°; the middle subpanel (II) shows the polarization pulse profiles, with lines indicating total intensity (black, normalized to a peak value of 1.0), linear polarization (red), and circular polarization (blue); and the bottom subpanel (III) shows the dynamic spectra (color bar). Error bars in each subpanel (I) indicate 1σ error for the polarization position angle.

For the alternative intrachannel depolarization, the fractional reduction in the linear polarization amplitude, f_{depol}, is defined as

$$f_{\mathrm{depol}} \equiv 1 - \frac{\sin(\Delta\theta)}{\Delta\theta} \qquad (1)$$

where $\Delta\theta$ is the intrachannel polarization position angle rotation. $\Delta\theta$ is defined as $\Delta\theta \equiv \frac{2\mathrm{RM}_{\mathrm{obs}}c^2\Delta\nu}{\nu_c^3}$, where $\mathrm{RM}_{\mathrm{obs}}$ is the observed rotation measure, c is the speed of light, $\Delta\nu$ is the channel frequency width, and ν_c is the cen-tral channel observing frequency. For repeat-ers, the measured RMs are too small to explain the depolarization through this effect (f_{depol} listed in tables S1 and S3). We infer that in-trachannel depolarization is unlikely to be a major cause of depolarization for repeating FRBs.

We next examine RM scattering, the dis-persion of RM about the apparent mean for each source (*23*). RM scattering can be caused by multipath transmission of signals in an inhomogeneous magneto-ionic environment.

If the scattering is sufficiently large, it can become substantial enough to depolarize the pulses, analogous to pulsar pulses passing through a stellar wind (*24, 25*). We parame-terize the depolarization due to RM scattering as (*23*)

$$f_{\mathrm{RM\ scattering}} \equiv 1 - \exp(-2\lambda^4\sigma_{\mathrm{RM}}^2) \qquad (2)$$

where $f_{\mathrm{RM\ scattering}}$ is the fractional reduction in the linear polarization amplitude, σ_{RM} is the
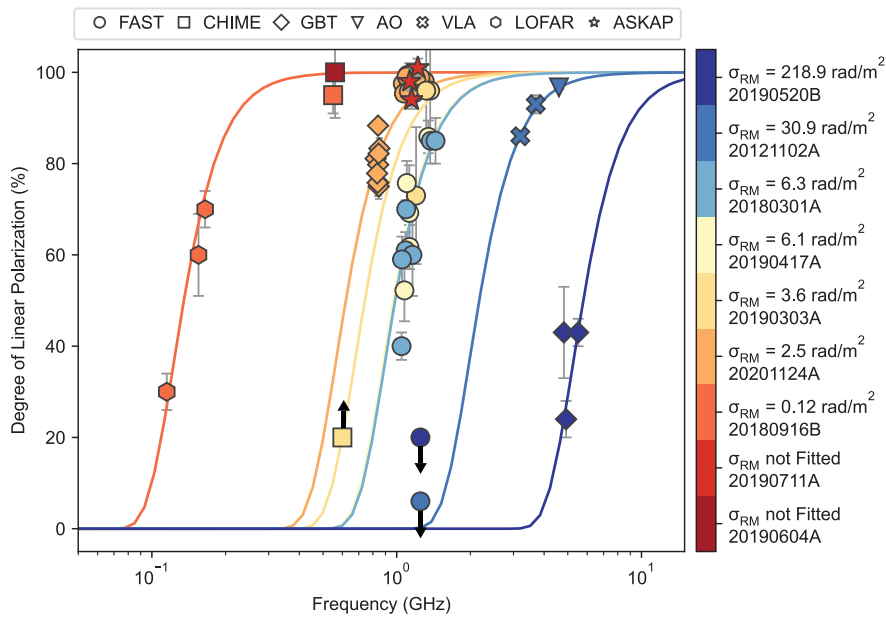
Fig. 2. The degree of linear polarization for FRB sources is consistent with RM scattering. Data points (with 1σ error bars) indicate the degree of linear polarization as a function of frequency for each FRB (indicated at right). The colored lines are models of emission that is intrinsically 100% linearly polarized, then depolarized by various σ_{RM} levels following the model in Eq. 2, fitted to each FRB separately. Arrows indicate 95% upper and lower limits. All bursts in the sample are consistent with an RM scattering model. Data values and sources are listed in tables S1 and S3; fitted σ_{RM} values are in table S2. Symbol shapes indicate the telescope used for each observation: Five-hundred-meter Aperture Spherical radio Telescope (FAST), Canadian Hydrogen Intensity Mapping Experiment (CHIME), Robert C. Byrd Green Bank Telescope (GBT), Arecibo Observatory (AO), Karl G. Jansky Very Large Array (VLA), Low-Frequency Array (LOFAR), and Australian Square Kilometre Array Pathfinder (ASKAP).
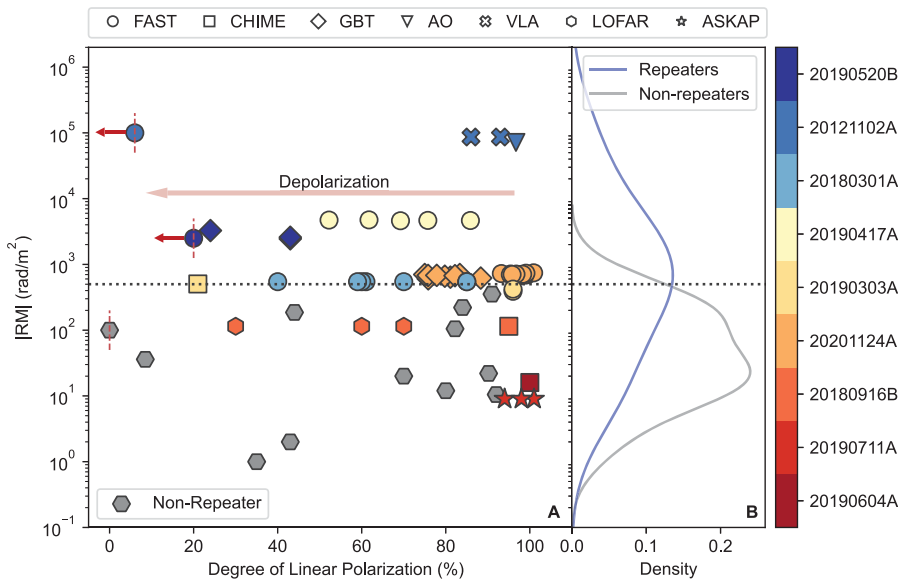
Fig. 3. Relationship between RM and degree of linear polarization. (**A**) Data for repeating (colored points) and nonrepeating FRBs (gray points). Symbol shapes and colors are the same as in Fig. 2. Vertical dashed red lines indicate nondetections of RM in the L band; thus, the associated data points are displayed at nominal values that are either representative or measured at higher frequencies: 100 rad/m² for FRB 20140514A, 3000 rad/m² for FRB 20190520B, and 10⁵ rad/m² for FRB 20121102A. Red arrows denote 95% upper limits on the linear polarization. The horizontal dotted black line, which lies above all nonrepeaters, indicates |RM| = 500 rad/m². (**B**) Kernel density estimation of the RMs for repeaters (blue line) and nonrepeaters (gray line). A Kolmogorov-Smirnov test between the repeaters and nonrepeaters finds a P value of 0.02, indicating that they are statistically different from each other.

standard deviation of the RM, and λ is the wavelength.

Depolarization at lower frequencies, consistent with irregular RM variations, has been seen in a few pulsars with scatter broadening. For example, the variable degree of linear polarization observed in the pulsar PSR J0742−2822 between 200 MHz and 1 GHz can be described by Eq. 2 with σ_{RM} = 0.13 rad/m² (26).

Complex magneto-ionic environments have previously been inferred from observations for some repeaters (8, 13). We also expect RM scatter for FRBs in such environments. In Fig. 2, we show the degree of linear polarization versus frequency for each source individually. Frequency evolution can be seen for all sources, but the depolarization occurs at different bands. FRB 20180916B is depolarized below 200 MHz (27), whereas FRB 20121102A (28) is depolarized at frequencies lower than 3.5 GHz. We fitted the data for each repeater using the model in Eq. 2, with a different σ_{RM} for each source (16). For the sources depolarized at lower frequencies (<200 MHz), such as FRB 20180916B, we derive σ_{RM} ~ 0.1 rad/m² (table S2). Such a small scatter is consistent with the environment being less turbulent, dense, and/or magnetized than that of other FRBs, as might be expected for an old stellar population (27). We find σ_{RM} ~ 2.5 rad/m² for FRB 20201124A, σ_{RM} ~ 3.6 rad/m² for FRB 20190303A, σ_{RM} ~ 6.1 rad/m² for FRB 20190417A, σ_{RM} ~ 6.3 rad/m² for FRB 20180301A, and σ_{RM} ~ 30.9 rad/m² for FRB 20121102A (table S2). The RM scatter of 30.9 rad/m² is consistent with FRB 20121102A originating in a younger stellar population (28) that produced an inhomogeneous magneto-ionic environment. For the repeater FRB 20190520B, which depolarizes at frequencies higher than 1 GHz, we derive σ_{RM} ~ 218.9 rad/m².

The observations are consistent with repeating bursts being intrinsically nearly 100% linearly polarized, then being depolarized during propagation, which can be characterized by the RM scatter parameter σ_{RM}. The same environment that gives rise to large σ_{RM} could also cause Faraday conversion, whereby linearly polarized light is converted to circularly polarized light, potentially explaining the circular polarization observed in some FRBs (29). We interpret the σ_{RM} values derived from our analysis as a measure of the complexity level of the magneto-ionic environments that host active repeaters, with larger σ_{RM} values possibly being associated with younger stellar populations.

Figure 3 shows the relation between RM and linear polarization for the repeating and nonrepeating FRBs in our sample that have polarization measurements. A Kolmogorov-Smirnov test between the repeaters and nonrepeaters shows that the RM distributions differ, indicating that they may reside in different
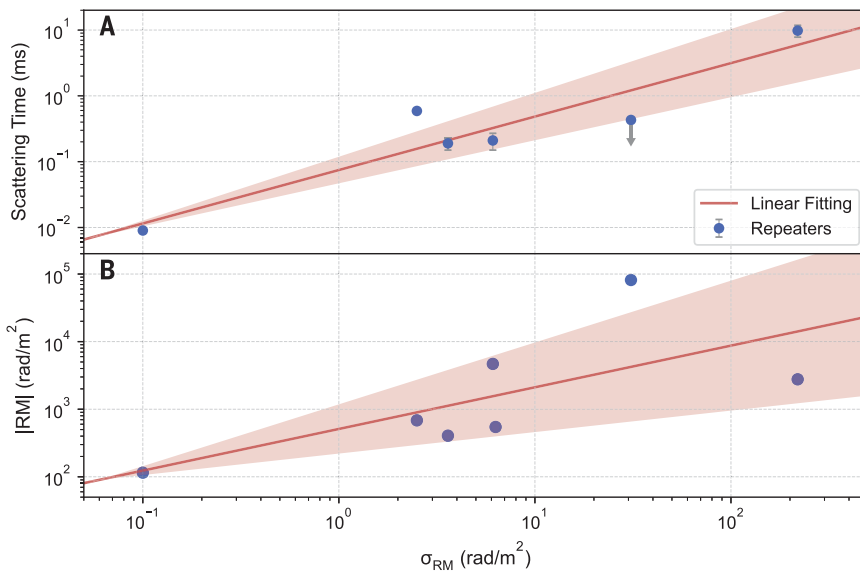
Fig. 4. Correlations between σ_{RM}, scattering time τ_{sca}, and rotation measure magnitude |RM| for repeating FRBs. (**A**) Relationship between σ_{RM} and scattering time scaled to 1300 MHz (*16*) for repeaters with σ_{RM} measurements (error bars, 1σ error for the scattering time). The data used are listed in table S2. FRB 20121102A is an upper limit (gray arrow). The Pearson product-moment correlation coefficient of $\log\tau_{sca}$ and $\log\sigma_{RM}$ is 0.47. Fitting the data with a linear model (red line) yields a slope of 0.81 ± 0.16. (**B**) Relationship between σ_{RM} and |RM| for the same sample of repeaters. The Pearson product-moment correlation coefficient of $\log|RM|$ and $\log\sigma_{RM}$ is 0.68. Fitting the data with a linear model (red line) yields a slope of 0.62 ± 0.30. All quantities are measured in the observer's frame. The 1σ uncertainties on σ_{RM} and |RM| are smaller than the symbol size.

environments. We caution that the intrachannel depolarization may introduce a selection bias if the nonrepeaters have systematically larger RMs, because discovery searches tend to use coarser filter banks than follow-up observations.

If σ_{RM} is due to multipath propagation effects on individual FRBs, we would expect the same effect to produce a temporal scattering in the pulse profile. In Fig. 4A, we show RM scatter and scattering time scales (listed in table S2) for our repeater sample. The two are positively correlated, consistent with the hypothesis that RM scatter and pulse scattering originate from a single plasma screen, such as a supernova remnant or pulsar wind nebula (*30*). σ_{RM} and |RM| are also positively correlated (Fig. 4B). In the context of our multipath-scattering model, this indicates that an environment with a stronger magnetic field strength *B* tends to have a larger fluctuation in *B*.

FRB 20190520B and FRB 20121102A are the only two FRBs known to have associated compact PRSs (*4*, *18*). We find that these two repeaters have the largest σ_{RM}. The combination of large RM (dense) and strong *B* field (magnetized) tends to produce large σ_{RM}. A denser and more magnetized environment likely also produces stronger synchrotron radiation from the nebula, resulting in a PRS (*31*), consistent with the multipath-scattering picture. Repeaters with large observed σ_{RM}

could be more affected by turbulence, resulting in large fluctuations of electron density and magnetic field, which may explain the diversity among repeaters (*30*).

In summary, repeating FRBs are less polarized at lower frequencies, which can be explained by an RM scatter model. The value of σ_{RM} in the model can be used to quantify the complexity of magnetized environments associated with repeating FRBs. High values of σ_{RM} possibly indicate sources in younger stellar populations.

REFERENCES AND NOTES

1. D. R. Lorimer, M. Bailes, M. A. McLaughlin, D. J. Narkevic, F. Crawford, *Science* **318**, 777–780 (2007).
2. L. G. Spitler *et al.*, *Nature* **531**, 202–205 (2016).
3. B. Zhang, *Nature* **587**, 45–53 (2020).
4. B. Marcote *et al.*, *Astrophys. J. Lett.* **834**, L8 (2017).
5. R. Luo, K. Lee, D. R. Lorimer, B. Zhang, *Mon. Not. R. Astron. Soc.* **481**, 2320–2337 (2018).
6. D. W. Gardenier, J. van Leeuwen, L. Connor, E. Petroff, *Astron. Astrophys.* **632**, A125 (2019).
7. J.-P. Macquart, R. D. Ekers, *Mon. Not. R. Astron. Soc.* **474**, 1900–1908 (2018).
8. D. Michilli *et al.*, *Nature* **553**, 182–185 (2018).
9. A. L. Piro, B. M. Gaensler, *Astrophys. J.* **861**, 150 (2018).
10. B. Margalit, B. D. Metzger, *Astrophys. J. Lett.* **868**, L4 (2018).
11. W. Lu, P. Kumar, R. Narayan, *Mon. Not. R. Astron. Soc.* **483**, 359–369 (2019).
12. S. Dai *et al.*, *Astrophys. J.* **920**, 46 (2021).
13. R. Luo *et al.*, *Nature* **586**, 693–696 (2020).
14. S. Chatterjee *et al.*, *Nature* **541**, 58–61 (2017).
15. D. Li *et al.*, *Nature* **598**, 267–271 (2021).
16. Materials and methods are available as supplementary materials.
17. D. Li *et al.*, *IEEE Microw. Mag.* **19**, 112–119 (2018).
18. C.-H. Niu *et al.*, arXiv:2110.07418 [astro-ph.HE] (2021).
19. E. Fonseca *et al.*, *Astrophys. J. Lett.* **891**, L6 (2020).
20. CHIME/FRB Collaboration, The Astronomer's Telegram no. 14497 (2021); www.astronomerstelegram.org/?read=14497.
21. S. Johnston, M. Kerr, *Mon. Not. R. Astron. Soc.* **474**, 4629–4636 (2018).
22. S. A. Petrova, *Astron. Astrophys.* **378**, 883–897 (2001).
23. S. P. O'Sullivan *et al.*, *Mon. Not. R. Astron. Soc.* **421**, 3300–3315 (2012).
24. X. P. You, R. N. Manchester, W. A. Coles, G. B. Hobbs, R. Shannon, *Astrophys. J.* **867**, 22 (2018).
25. E. J. Polzin *et al.*, *Mon. Not. R. Astron. Soc.* **490**, 889–908 (2019).
26. M. Xue *et al.*, *Publ. Astron. Soc. Aust.* **36**, e025 (2019).
27. Z. Pleunis *et al.*, *Astrophys. J. Lett.* **911**, L3 (2021).
28. G. H. Hilmarsson *et al.*, *Astrophys. J. Lett.* **908**, L10 (2021).
29. G. H. Hilmarsson, L. G. Spitler, R. A. Main, D. Z. Li, *Mon. Not. R. Astron. Soc.* **508**, 5354–5361 (2021).
30. Detailed modeling and discussions can be found in the supplementary text.
31. Y.-P. Yang, Q.-C. Li, B. Zhang, *Astrophys. J.* **895**, 7 (2020).
32. D. Li, Frequency dependent polarization of repeating fast radio bursts - implications for their origin, version 4, Science Data Bank (2022); https://doi.org/10.11922/sciencedb.o00069.00006.

Science

Frequency-dependent polarization of repeating fast radio bursts—implications for their origin

Yi FengDi LiYuan-Pei YangYongkun ZhangWeiwei ZhuBing ZhangWenbin LuPei WangShi DaiRyan S. LynchJumei YaoJinchen JiangJiarui NiuDejiang ZhouHeng XuChenchen MiaoChenhui NiuLingqi MengLei QianChao-Wei TsaiBojun WangMengyao XueYouling YueMao YuanSongbo ZhangLei Zhang

Polarized repeating fast radio bursts

Fast radio bursts (FRBs) are intense, millisecond flashes of radio emission from extragalactic sources of unknown origin. Most FRBs are seen only once, but others repeat at irregular intervals and thereforre can be followed. Feng *et al.* measured the polarization of five repeating FRBs (see the Perspective by Caleb). They found that each source is polarized at high frequencies but becomes depolarized below a threshold frequency that varies between sources. The authors found that all repeating FRBs are 100% polarized at the source, before the radio waves scatter off complex foreground structures such as supernova remnants. These results constrain theories of the repeating FRB emission mechanism. —KTS

View the article online
https://www.science.org/doi/10.1126/science.abl7759
Permissions
https://www.science.org/help/reprints-and-permissions

Use of this article is subject to the Terms of service